BILINGUAL PUBLISHING GROUP

Journal of Atmospheric Science Research

https://journals.bilpubgroup.com/index.php/jasr/index

ARTICLE

Multi-decadal Changes of the Impact of El Niño Events on Tibetan Plateau Summer Precipitation

***Weinan Jiang*[1,2,3], *Ning Cao*[1,2,3,4*], *Riga Aze*[1,2,3], *Jianjun Xu*[2,3,4]**

[1] *College of Ocean and Meteorology, Guangdong Ocean University, Zhanjiang, Guangdong, 524088, China*

[2] *CMA-GDOU Joint Laboratory for Marine Meteorology, Guangdong Ocean University, Zhanjiang, Guangdong, 524088, China*

[3] *South China Institute of Marine Meteorology (SIMM), Guangdong Ocean University, Zhanjiang, Guangdong, 524088, China*

[4] *Shenzhen Institute of Guangdong Ocean University, Shenzhen, Guangdong, 518108, China*

ABSTRACT

Precipitation on the Tibetan Plateau (TP) has an important effect on the water supply and demand of the downstream population. Involving recent climate change, the multi-decadal variations of the impact of El Niño-Southern Oscillation (ENSO) events on regional climate were observed. In this work, the authors investigated the changes in summer precipitation over TP during 1950–2019. At the multi-decadal scale, the authors found that the inhabiting impact of El Niño events on the TP summer precipitation has strengthened since the late 1970s. The main factor contributing to this phenomenon is the significant amplification in the decadal amplitude of El Niño during 1978–2019 accompanied by a discernible escalation in the frequency of El Niño events. This phenomenon induces anomalous perturbations in sea surface temperatures (SST) within the tropical Indo-Pacific region, consequently weakening the atmospheric vapor transport from the western Pacific to the TP. Additionally, conspicuous anomalies in subsidence motion are observed longitudinally and latitudinally across the TP which significantly contributes to a curtailed supply of atmospheric moisture. These results bear profound implications for the multi-decadal prediction of the TP climate.

Keywords: Tibetan plateau; Summer precipitation; ENSO; Multi-decadal changes; Climate variability

*CORRESPONDING AUTHOR:

Ning Cao, College of Ocean and Meteorology, Guangdong Ocean University, Zhanjiang, Guangdong, 524088, China; CMA-GDOU Joint Laboratory for Marine Meteorology, Guangdong Ocean University, Zhanjiang, Guangdong, 524088, China; South China Institute of Marine Meteorology (SIMM), Guangdong Ocean University, Zhanjiang, Guangdong, 524088, China; Shenzhen Institute of Guangdong Ocean University, Shenzhen, Guangdong, 518108, China; Email: ncao@gdou.edu.cn

ARTICLE INFO

Received: 27 December 2023 | Revised: 24 January 2024 | Accepted: 26 January 2024 | Published Online: 31 January 2024

DOI: https://doi.org/10.30564/jasr.v7i1.6180

CITATION

Jiang, W.N., Cao, N., Aze, R., et al., 2024. Multi-decadal Changes of the Impact of El Niño Events on Tibetan Plateau Summer Precipitation. Journal of Atmospheric Science Research. 7(1): 90–105. DOI: https://doi.org/10.30564/jasr.v7i1.6180

1. Introduction

The Tibetan Plateau (TP) lies between 25°N and 45°N, 65°E and 105°E. It constitutes the world's largest Plateau, covering an area of 2.5 million square kilometers that extends from the Pamir Plateau in the west to the Hengduan Mountains in the east; and from the Kunlun Mountains and Qilian Mountains in the north to the Himalaya Mountains in the south [1]. The Tibetan Plateau also includes the highest land mass, with an average elevation of over 4500 meters. It forms one of the major drivers of global climate, referred as the Earth's "third pole" [2]. The TP area is recognized as the "Asia Water Tower" due to its location within Asia, where it plays a vital role in supplying water to numerous river networks [3]. Precipitation patterns in the region have been considered to be affected by climate change, with further impacts on the ecological environment and human society [4]. For example, changes in precipitation patterns not only influence vegetation distribution, consequently shaping the ecological environment [5], but also induce modifications in river flow, thereby exerting effects on downstream agriculture [3]. The latent heat released during precipitation can drive atmospheric circulation and further affect the climate of East Asia [6–8]. Summer precipitation over the TP accounts for more than 60% of the total annual precipitation [9]. Therefore, it is important for water resource variations and people's life to investigate the summer precipitation over the TP.

The primary factor influencing precipitation variations on the TP is the large-scale atmospheric circulation, the interaction between the westerlies and monsoons stands out as a key mechanism affecting water vapor transport and precipitation distribution in the TP region [10,11]. The westerlies transport moisture from the Mediterranean-Iran Plateau region to the TP and the moisture in the southern TP primarily comes from monsoons [12], changes in the westerlies and monsoons inevitably lead to variations in the TP climate. Alongside global climate warming and changes in the atmospheric circulation model, the precipitation on the Tibetan Plateau has also changed. Of course, there are many factors that affect precipitation on the TP [13–15], and changes in sea surface temperature (SST) are one of them. As the strongest signal in the air-sea interaction system, the influence of El Niño-Southern Oscillation (ENSO) on precipitation cannot be ignored.

During El Niño, SST significantly rises in the eastern Pacific, while in La Niña the opposite occurs. The influence of El Niño on TP precipitation is usually indirect, El Niño induces changes of SST in other ocean basins and atmospheric circulation to affect TP precipitation. For example, El Niño can induce SST anomalies in the Indian Ocean and North Atlantic [16–20], which affect TP summer precipitation through the Indo-western Pacific Ocean capacitor [17,21] effect and atmospheric circulation. To elaborate, during the 3–6 months following the peak of El Niño, the SST in the Indian Ocean and the tropical North Atlantic Ocean become warmer than normal [16], and the land-sea thermal contrast between the Eurasian continent and the Indian Ocean weakens. Furthermore, El Niño induced Indian Ocean SST anomaly and led to an anti-symmetric pattern of atmospheric anomalies in the tropical north Indian Ocean [22], which delayed the onset of the Indian monsoon and reduced early summer precipitation in the TP [23]. As El Niño decays during the summer, the Indo-western Pacific Ocean capacitor effect sustains the warming of SST in the tropical North Indian Ocean [21], thus maintaining the impact of ENSO on TP summer precipitation. With regard to the North Atlantic SST, El Niño can trigger a tripolar SST pattern in the North Atlantic, a phenomenon that often persists into the summer [24]. This tripolar pattern exerts a remote influence on the summer precipitation in the Tibetan Plateau through teleconnections [25]. These mechanisms determine that the impact of El Niño's effects persist not only during the development year of ENSO but even in the year following its peak [26].

Many studies have shown that the developing phase of El Niño can weaken TP summer precipitation [27–29]. In recent decades, the structure of

ENSO has experienced interdecadal changes [30,31], with frequent Central-Pacific El Niño events and increasing intensity [32–34], the duration of SST anomalies in the Central Pacific caused by El Niño is also longer than in the past [35]. This means that the regional climate system related to ENSO is undergoing interdecadal changes [19,36–38], including TP summer precipitation. Then the question arises: What decadal changes have occurred in the relationship between El Niño and TP summer precipitation? The objective of the present study is to reveal the TP summer responses to the interdecadal change of ENSO, and to feature corresponding changes of water vapor transport over TP and the surrounding plateau-monsoon regions.

2. Materials and methods

The global land surface precipitation data used in this work are from version 4.05 of the CRU TS monthly high-resolution gridded climate dataset [39], produced by the UK's National Centre for Atmospheric Science (NCAS) at the University of East Anglia's Climatic Research Unit (CRU). It has a horizontal resolution of 0.5° × 0.5°, covering the period 1901–2020. The CRU-TS4.05 data comprises monthly gridded fields based on monthly observational data calculated from daily or sub-daily data by National Meteorological Services and other external agents.

In contrast, total precipitation data from the reanalysis dataset ERA5 are also used to validate the results derived from CRU-TS4.05 data. The vertical integral of water vapor flux, total column water vapor, and vertical velocity data are all from the ERA5 product, downloaded from the Climate Data Store (CDS). ERA5 is the fifth-generation ECMWF reanalysis for global climate and weather, with a horizontal resolution of 0.25° × 0.25° and 37 levels in the vertical direction for atmosphere reanalysis. It is available from 1940 [40], with a large number of observations assimilated into the numerical weather forecasting model to obtain a consistent dataset constrained by the laws of physics [41]. In this work, we use the ERA5 product for the period 1950 to 2019.

The SST used in this work is from the Hadley Centre Sea Ice and Sea Surface Temperature dataset (HadISST) [42]. The monthly index of ENSO is specified as the area-averaged SST from the Niño-3.4 region (5°S–5°N and 170–120°W, anomaly with the 1981–2010 mean removed) using the HadISST1 dataset, hereafter the Niño-3.4 index. The study period is denoted as 1950–2019 according to the time ranges of these datasets. If not specifically specified, the seasonal mean is defined as March-April-May mean for spring, June-July-August mean for summer, September-October-November mean for autumn, and December-January-February mean for winter, according to the boreal season cycle. Additionally, we use (0) to denote the year of TP summer we focused on, (–1) to denote the former year, and (1) to denote the following year. ENSO is phase-locked to the annual cycle. Typically, eastern Pacific (Niño-3.4) SST anomalies begin to develop in JJA(0), peak in D(0)JF(1), and decay rapidly in MAM (1). The developing stage denotes JJA(0) to D(0)JF(1), while the decaying stage denotes D(0)JF(1) to MAM(1).

Using the Pearson R statistical test, we analyze the correlation between ENSO and summer precipitation on the plateau. Additionally, we observe its variations through a 21-year sliding correlation analysis (comprising the preceding 10 years, the current year, and the subsequent 10 years). As we investigate the interdecadal to multi-decadal change in the interannual relationship, all data are linearly detrended. The statistical significance is tested via the two-tailed Student's *t* test.

3. Results

3.1 TP summer precipitation and its changes

Using monthly precipitation data from the observation-determined product of the global land surface precipitation dataset CRU-TS4.05 and the widely used ERA5 products from the fifth-generation ECMWF reanalysis system, we present the 70-year mean summer precipitation (1950–2019) in **Figures 1a–1b**. In both datasets, patterns of "wet in southeast TP and dry in north and west TP" are observed. It

is evident that summer precipitation mainly occurs in the south and southeast parts of TP for multi-year means, with an average daily precipitation of 5–8 mm at the southern edge of the plateau. The summer precipitation in northern and western TP is less than 2 mm/day. A magenta rectangle in (a, b) was drawn to denote the area of southeast TP (SETP, 85°–105°E, 25°–35°N). Based on the CRU data for 1950–2019, summer precipitation over the SETP region accounts for about 70% of that over the entire TP region. For the regional mean, SETP has 4.0 mm/day precipitation averaged in summer, which is nearly twice the TP mean summer precipitation (2.4 mm/day). The time series of TP and SETP mean summer precipitation are shown in **Figures 1c–1d**.

The TP mean summer precipitation is associated with ENSO, with the correlation coefficient reaching –0.40 and –0.31 between the summer Niño-3.4 index (bars in the figure) and the TP mean series for CRU-TS4.05 and ERA5, respectively (**Figure 1c**), exceeding a 99% confidence level. The SETP mean summer precipitation also correlates with the summer Niño-3.4 index with coefficients of –0.30 and –0.14 for CRU-TS4.05 and ERA5 (**Figure 1d**), but only the CRU result exceeds the 98% confidence level, while the ERA5 result is less than 80%. In fact, although precipitation over the SETP region accounts for about 70% of that over the entire TP region, the dominant significant negative correlations lie in the region of south and south-west of TP, rather than the rectangle region of SETP, as is shown in **Figure 3** with the patterns of correlation coefficients. Therefore, we designate the time series of TP mean summer precipitation as an index to represent the changes in TP precipitation in the following correlation and regression analyses.

3.2 TP summer precipitation and its changes

To highlight the relationship between TP summer precipitation and ENSO, we present the lead-lag correlation coefficients of TP mean summer precipitation (shown in **Figure 1c**) and the monthly Niño-3.4 index in a 3-year cycle during 1950–2019, using CRU-TS4.05 and ERA5 precipitation data in **Figure 2a**. At a 95% confidence level, both datasets show that TP mean summer precipitation negatively correlates with the Niño-3.4 index from spring(0) to spring(1), indicating that the variability of TP summer(0) precipitation is consistent with the variabilities of ENSO during its life-cycle from onset in spring(0) to dying out in spring(1).

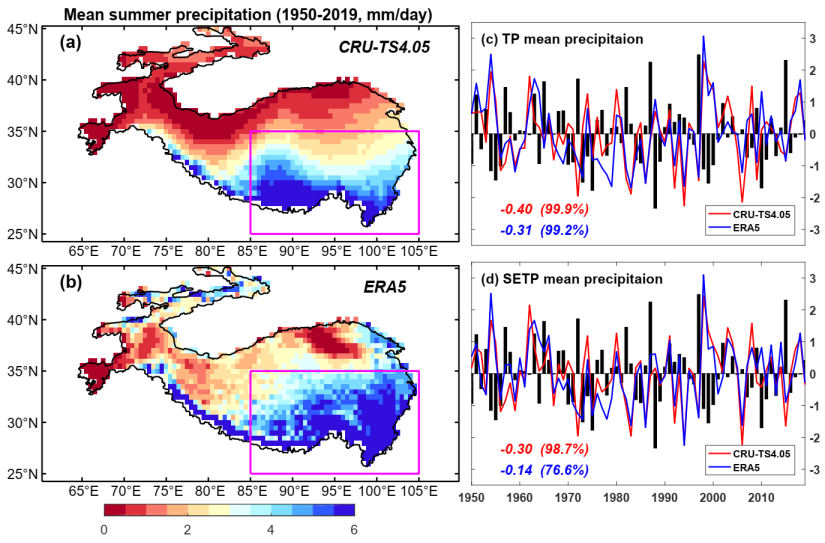

Figure 1. Mean summer precipitation over Tibetan Plateau during 1950–2019 using data from (a) CRU TS4.05 and (b) ERA5 products, and the time series of the normalized (c) TP mean and (d) SETP mean summer precipitation derived by CRU-TS4.05 (red line) and ERA5 (blue line) products and the normalized concurrent summer Niño-3.4 index (bars). The magenta rectangle in (a, b) denotes the area SETP. The correlation coefficients between the precipitation time series and the Niño-3.4 index are shown on the bottom with the confidence levels in parentheses. All time series have been linearly detrended.

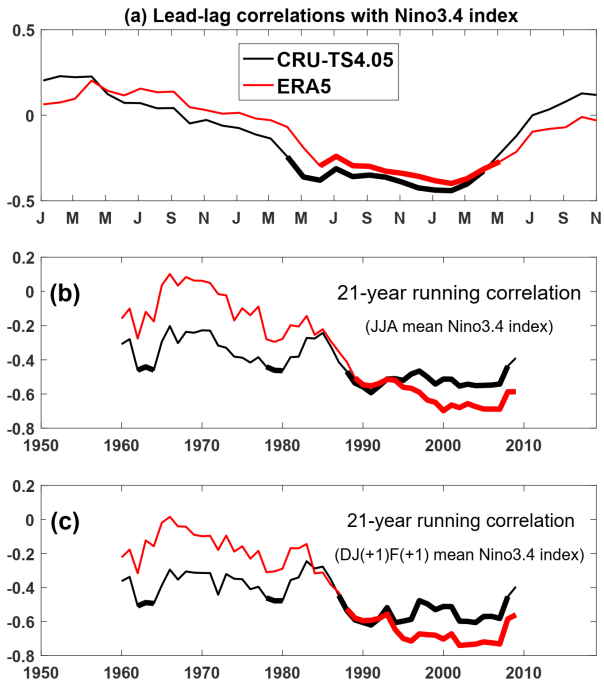

Figure 2. (a) Lead-lag correlation coefficients of TP mean summer precipitation and the monthly Niño-3.4 index in 3-year cycle during 1950–2019; (b) The 21-year running correlation of TP mean summer precipitation and the JJA mean Niño-3.4 index; (c) Same as (b), but for the DJ(+1)F(+1) mean Niño-3.4 index. The notation (+1) denotes the year after the ENSO event. Results of CRU-TS4.05 and ERA5 data are shown in black and red lines. The correlation is shown at the center year of the 21-year window. Bold lines indicate correlation coefficients exceeding 95% confidence level.

Based on this result, we focused our attention on the impact of ENSO on TP summer climate in the developing stage and examined the interdecadal change in the relationship between the two series. Here we introduce a method of running correlations with a 21-year window. **Figures 2b–2c** present the results of a 21-year running correlation between the normalized TP mean summer precipitation and Niño-3.4 index for JJA(0) mean and D(0)JF(1) mean, respectively. It is evident that the relationship between them has experienced an interdecadal change since the late 1980s, precisely since 1988 for CRU and since 1989 for ERA5, at the 95% confidence level. As the correlation is shown at the center year of the 21-year window, taking 1989 as an example, it represents the relations of the two for the 1979–1999 period. So if the transition from insignificant to significant occurred since 1989, it means that any 21-year period after the year 1979 will show a significant correlation.

Both the concurrent summer Niño-3.4 index and the mature phase winter Niño-3.4 index show consistent results, and the two precipitation datasets also support each other. As the 21-year running correlation coefficient was statistically significant since 1988/1989 (the result for the period of 1978–1998/1979–1999), we can conclude that relations between TP summer precipitation and ENSO have exhibited an interdecadal abrupt change and become statistically significant in recent decades, suggesting a strengthened relationship between TP mean summer precipitation and ENSO since the late 1970s. Thus, we choose 1950–1978 (P1) and 1979–2019 (P2) as the two sub-periods in the following correlation and regression analyses to understand the different relationships between TP summer rainfall and tropical Indo-Pacific SST variabilities. Obviously, the two sub-periods respectively represent insignificant and significant correlations between TP summer precipitation and ENSO in its developing stage.

Figure 3 presents patterns of correlation coefficients of TP summer precipitation derived from CRU and ERA5 data with the summer mean Niño-3.4 series for the whole period 1950–2019 and the divided sub-periods of 1950–1978 (P1) and 1979–2019 (P2). It is evident that the most significant correlation coefficient center is located in southwest TP, consistent with a previous study [28], but the patterns for the two sub-periods show some remarkable differences. During 1950–1978, the patterns mainly show negative correlations at southwest TP (significant) and positive at north-central-southeast parts (mostly insignificant). The impact of ENSO on southwest TP can be considered a part of the Indian summer monsoon system, indicating that El Niño events in their developing years will significantly weaken the summer monsoon and bring less precipitation in the Indian subcontinent, while La Niña event effects are the opposite. However, during 1979–2019, the location of negative correlations

expands eastward, making a dramatic decrease in the positive correlations at north-central-southeast TP. As stated above, for the 1950–2019 climatology, SETP accounts for about 70% of the entire TP summer precipitation. In 1950–1978, although the positive correlations at north-central-southeast TP are not statistically significant, they can generally offset the negative correlations at SWTP, causing insignificant correlations between entire TP mean summer precipitation and ENSO (**Figure 2b**). In contrast, during 1979–2019, the positive correlations at north-central-southeast TP have greatly weakened and even become negative. Meanwhile, the significant negative correlations have expanded to central-southeast TP, causing significant correlations between the entire TP mean summer precipitation and ENSO (**Figure 2b**). By investigating the ENSO-related summer precipitation over a larger region (known as monsoon Asia), in the former period, ENSO mainly impacts the north of the Indian subcontinent and southwest of TP negatively, while the correlation is relatively weak and insignificant in the south of India and central and east China. In contrast, for the later period, ENSO negatively correlates with summer precipitation in south India, south-central TP, east TP, and central China at a 90% confidence level. The comparisons led us to confirm that ENSO's impact on summer precipitation in central-southeast TP has significantly strengthened after 1979.

4. Possible mechanisms for interdecadal change

As shown above, the relationship between ENSO and TP summer precipitation has experienced an interdecadal change since the late 1970s. In this section, we further investigate the possible mechanisms for this interdecadal change by starting with a further contrast of the correlation of TP summer precipitation with SST before and after the late 1970s. There seems to be no distinct interdecadal change in the annual variation of TP mean summer precipitation in the 1970s, either for mean summer precipitation over the entire TP or for that over SETP (**Figures 1c–1d**). Therefore, the possible reasons for such interdecadal change in their correlations probably lie in the following two factors: the change of ENSO intensity or the pattern change of the contemporaneous SST in the tropical Indo-Pacific domain.

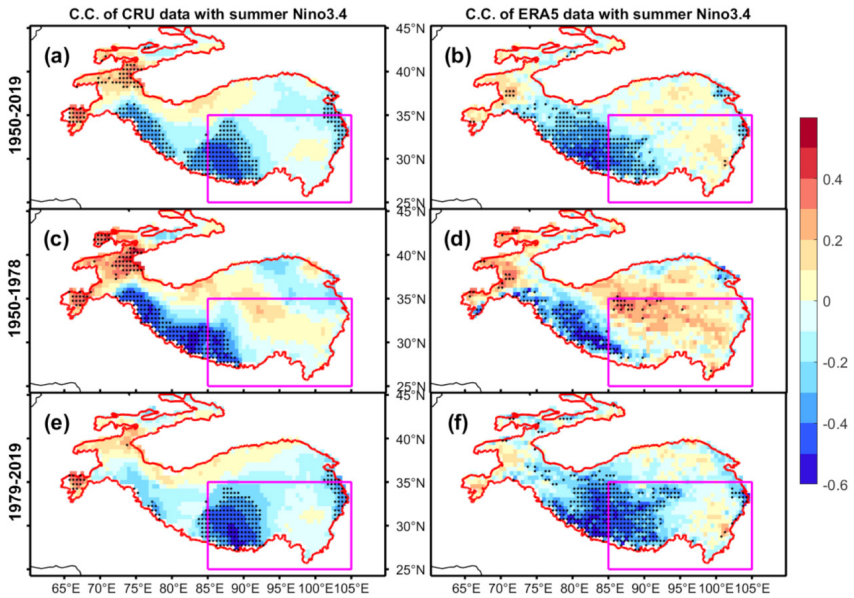

Figure 3. Patterns of correlation coefficients (C.C.) of summer precipitation derived from CRU (a, c, e) and ERA5 (b, d, f) data with summer Niño-3.4 series, for (a, b) the whole period 1950–2019, and the divided periods of (c, d) 1950–1978, (e, f) 1979–2019. The dotted areas indicate correlation coefficients exceed 90% confidence level. All data has been detrended to remove the effect of global warming.

4.1 Interdecadal change in relations between TP summer precipitation and ENSO

Firstly, the change of ENSO intensity is considered. Since the Niño-3.4 index captures the SST anomalies averaged generally over the maximum SST anomalies region, and the variations of SST are well phase-locked with the annual cycle, we can assign the D(0)JF(1) mean Niño-3.4 index as the amplitude of ENSO events, and the standard deviation of Niño3.4 index can be used to denote the intensity of ENSO. By using a 21-year sliding analysis method, the running standard deviation (STD) of the D(0)JF(1) mean Niño-3.4 index is shown in **Figure 4**, along with the running correlation series, similar to **Figure 2c**. With correlation coefficients of –0.61 and –0.54, both CRU and ERA5 data show significant negative correlations (exceeding a 95% confidence level) of changes in 21-year running STD and 21-year running correlations between ENSO and TP summer precipitation. These results show that the interdecadal change in the relationship between ENSO and summer TP precipitation can be determined by the strengthening of ENSO amplitude since the late 1970s, as the running STDs of the D(0)JF(1) mean Niño-3.4 index experienced a distinct increase at about the same time (mid-1970s) when the running correlation series jumped from negatively insignificant to negatively significant (late 1970s).

This interdecadal change in ENSO intensity may be considered as a result of modulation by the Atlantic multi-decadal oscillation (AMO) [43]. The AMO was in its negative phase from the 1970s through 2000, causing strengthened ENSO variability. It is worth noting that the AMO has changed to a positive phase since the 2000s, and the related ENSO amplitude may be weakened during the 2010s according to this theory. Whether it indicates a forthcoming interdecadal change in relations between ENSO and TP summer precipitation is a question that needs further investigation, as shown in **Figures 2 and 4**, where the 21-year running correlations also show that it will change from significant to insignificant.

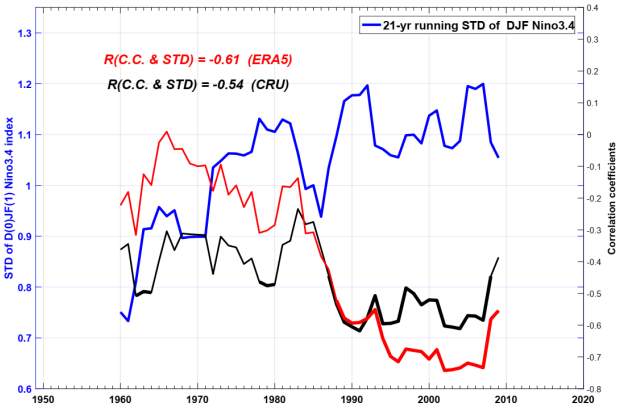

Figure 4. The 21-year running standard deviation of D(0)JF(1) mean Niño-3.4 index (STD, blue line), and the 21-year running correlation series same as **Figure 2c** (black and red lines). Bold black and red lines indicate correlation coefficients exceeding 95% confidence level.

4.2 Changes in ENSO patterns

Secondly, the pattern changes of the contemporaneous SST in the tropical Indo-Pacific domain are also examined by performing regression of tropical SST anomalies on the TP mean summer (JJA(0)) precipitation. The lead-lag regressions of seasonal mean SST onto TP mean summer precipitation, which show the results of seasonal evolution in the tropical Indo-Pacific oceans, are shown in **Figure 5**, from MAM(0)/spring to D(0)JF(1)/winter for two sub-periods.

Apparently, the SST anomalies related to TP summer precipitation in the tropical Indo-Pacific region are quite different between the two sub-periods. They generally show La Niña-like SST gradients for both sub-periods during an annual cycle, but the TP summer precipitation-related SST changes are much stronger in the later period than in the former period. In spring, the significantly related region includes the west Pacific (positive) and eastern equatorial Pacific (negative) in the former period, while in the later period as a contrast, the positive SST anomalies in the western Pacific greatly extend to the subtropical south and north Pacific, and the negative SST anomalies appear in central and northeastern equatorial Pacific. Over time, in the former period, the negative SST anomalies have

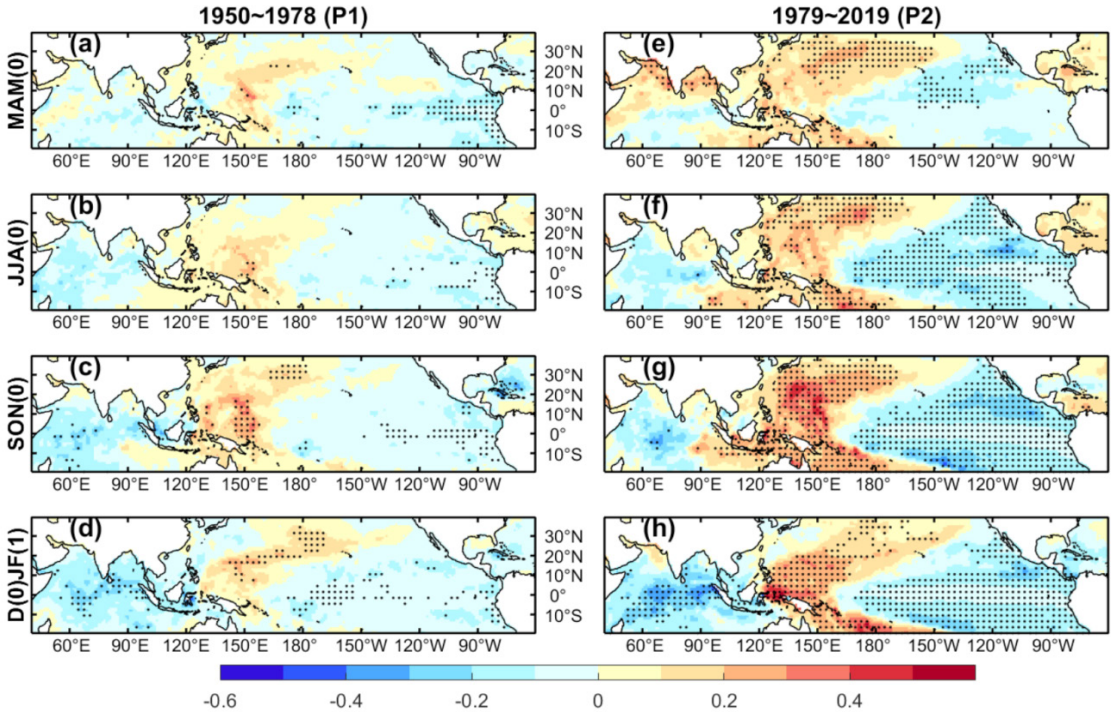

Figure 5. Lead-lag regressions of seasonal mean SST onto the TP mean summer precipitation for (a)–(d) period of 1950–1978 and (e)–(h) period of 1979–2019. Seasonal mean SSTA is for MAM(0), JJA(0), SON(0), and D(0)JF(1), respectively. Numerals 0 and 1 denote the simultaneous year and 1-year lag. The dots denote values exceeding the 95% confidence level. The SST data is derived from HadISST product and has been detrended.

greatly weakened in the eastern equatorial Pacific while the positive anomalies do not change much. By contrast, in the later period, the negative SST anomalies have greatly strengthened from spring to winter, with extraordinary positive-negative (or west-east) contrast covering almost the entire Pacific. The differences in TP summer precipitation-related SST anomalies patterns indicate that the relationship between TP summer precipitation and eastern equatorial Pacific SST anomalies has greatly strengthened in the later period relative to the former period.

Vastly different SST anomalies are also seen in the tropical Indian Ocean, which is considered to exhibit a season-dependent characteristic [44], that is, the SST anomaly is controlled by the Indian Ocean Dipole (IOD) mode during JJA and SON, and by Indian Ocean Basin wide (IOB) mode in DJF and MAM. The TP summer precipitation-related SST anomalies in the former period show no distinct IOD or IOB mode. However, in the later period, the related SST anomalies show a distinct IOD mode during JJA and SON, and IOB mode during MAM and DJF, which agrees pretty well with the season-dependent characteristic.

To investigate the differences in how the El Niño event impacts TP summer precipitation by affecting the water vapor transport during two sub-periods, a composite analysis is conducted. Here, we select the years of the El Niño developing stage and list them in **Table 1**. It was simply classified as an El Niño event if the D(0)JF(1) mean Niño-3.4 index exceeded half a standard deviation during the 1950–2019 period. There are 8 years in the period of 1950–1978, and 14 years in the period of 1979–2019 being selected as developing years of El Niño events.

Table 1. Selected years of El Niño developing stage for the divided two sub-periods.

Periods	Developing years of el niño events
1950–1978 (P1)	1957 1963 1965 1968 1969 1972 1976 1977
1979–2019 (P2)	1979 1982 1986 1987 1991 1994 1997 2002 2004 2006 2009 2014 2015 2018

Composite results of seasonal evolution mean SST anomalies for El Niño developing years over the tropical Indo-Pacific Ocean for periods of 1950–1978 and 1980–2019 are presented in **Figure 6**, from MAM(0)/spring to D(0)JF(1)/winter. Moreover, it should be noted that there were three super strong El Niño events in the later period, which occurred in 1982–1983, 1997–1998, and 2014–2016. To remove the influence of strong El Niño events, we delete these two years when using composite analysis in this figure. In the period of 1950–1978, the positive SST anomalies in the tropical Pacific developed from spring to autumn, featuring a maximum warming center located in the eastern region (**Figures 6a–6d**). In the later period 1979–2019, the warm SST anomalies in the tropical Pacific developed in summer and turned stronger in autumn, featuring a maximum warming center located in the central region (**Figures 6e–6h**). Such distinct differences suggest that the impacts of El Niño on the Asian summer climate during the two sub-periods are different.

4.3 Changes in water vapor transport

Summer precipitation on the TP has been largely determined by moisture supply from the oceans, including the Indian Ocean, and western Pacific, and even by the cross-equatorial flow from the southern hemisphere [45]. The differences in atmospheric water vapor transport in the two sub-periods may tell us how the strengthened ENSO impacts the precipitation in TP and surrounding plateau-monsoon regions.

As a contrast, **Figure 7** shows the composite of MAM(0), JJA(0), SON(0), D(0)JF(1) mean sea surface temperature anomalies (shaded) and vertical integral of vapor flux anomalies (vector) for El Niño developing years over the tropical Indo-Pacific Ocean for periods of 1950–1978 and 1979–2018 without removing the super 1982–1983, 1997–1998, 2014–2016 events. It is evident that the three super events make the composite SST anomalies pattern in the later period fairly stronger. The result that the amplitude of the anomalous SST during a life-cycle of El Niño event in the later period is larger than that in the former period indicates the amplitude of El Niño events has increased since the 1970s. Meanwhile, the anomalous eastward water vapor fluxes during a life-cycle of El Niño event are also stronger in the later period. El Niño events in the former period show the maximum SST anomalies appearing in the equatorial eastern Pacific, with anomalous equatorial eastward vapor flux over

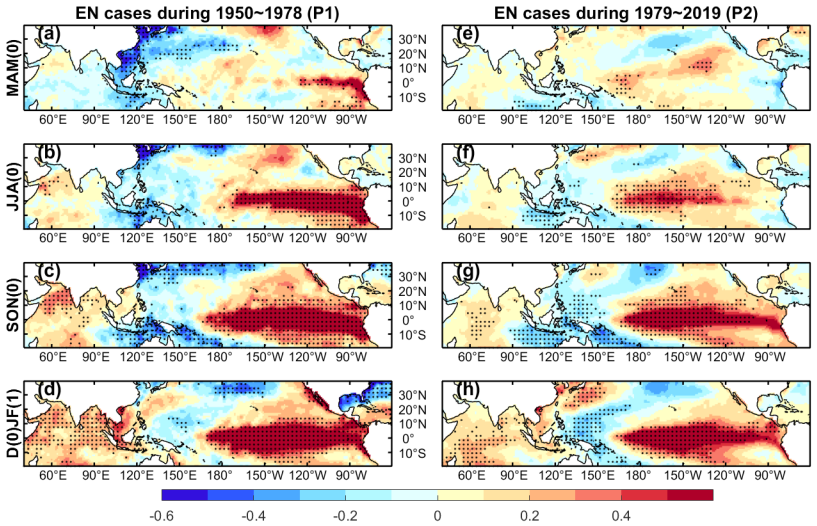

Figure 6. Composite of MAM(0), JJA(0), SON(0), D(0)JF(1) mean sea surface temperature anomalies for El Niño developing years (1982–1983, 1997–1998, 2014–2016 events are removed) during periods of 1950–1978 (left panel) and 1979–2019 (right panel). The dotted areas indicate composite mean SST anomalies exceed 95% confidence level. The SSTA data are derived from HadISST product and has been detrended.

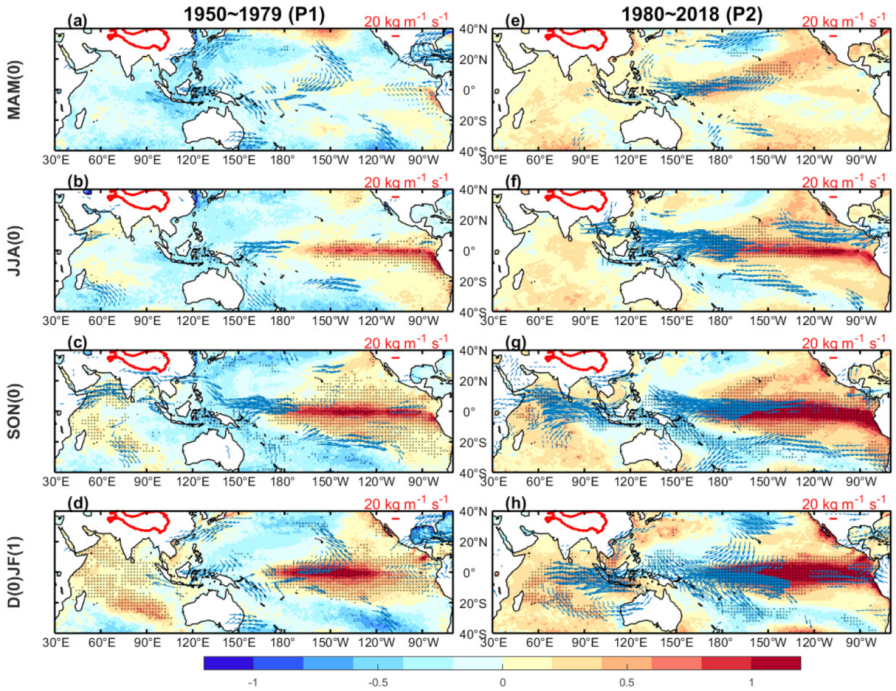

Figure 7. Same as **Figure 6**, but for composition including 1982–1983, 1997–1998, 2014–2016 events, and the concurrent vapor transport anomalies are shown.

the longitude range of 150°E–180°. In the later period, El Niño events show the initial maximum SST anomalies in spring appearing in the central Pacific and extra-equatorial of eastern Pacific and extending to central and eastern Pacific, with much stronger equatorial eastward anomalous vapor flux from 130°E to 150°W. The quantitative analysis on the detailed impact of three super El Niño events of 1982–1983, 1997–1998, and 2014–2016 events should be further investigated.

Considering the monsoon Asia region covering the TP and surrounding plateau-monsoon regions, **Figure 8** shows the composite anomalies of JJA(0) mean total column water vapor and vertical integral of vapor flux for El Niño developing years in the Large Triangular Sector of the plateau-monsoon region (TP-LTS) for the two sub-periods. In the former period, the significant anomalous water vapor flux appears in the northwest of the Indian Peninsula, with an anomalous anticyclone and strong anomalous vapor transport taking water vapor from the Indian Peninsula and Arab Sea to Africa. In the later period, significant anomalous water vapor flux appears in the Asia-Pacific region, with large amounts of water vapor being taken from the south and east of Asia, including the TP surrounding regions, to the tropical Pacific. An anomalous cyclone forms over the region surrounding Bengal, gathering much vapor over the Indo-China Peninsula. Meanwhile, the southward flow from north China to Beibu Gulf meets the eastward flow over the South China Sea, bringing large amounts of water vapor to southern China. This can well explain the correlation pattern shown in **Figure 3** and is consistent with the previous study.

4.4 Changes in vertical motion of air

Except for the horizontal transport of water vapor, the large-scale topography force can also reflect the vapor transport into or out of TP. So we examine the vertical structure of air motion during El Niño developing summer using ERA5 vertical velocity data. The negative (positive) values of vertical velocity indicate upward/ascent (downward/subsidence) air motion in the ERA5 dataset.

Figure 9 shows the latitude-pressure profiles of composite anomalies of JJA(0) mean vertical velocity for El Niño developing years averaged in

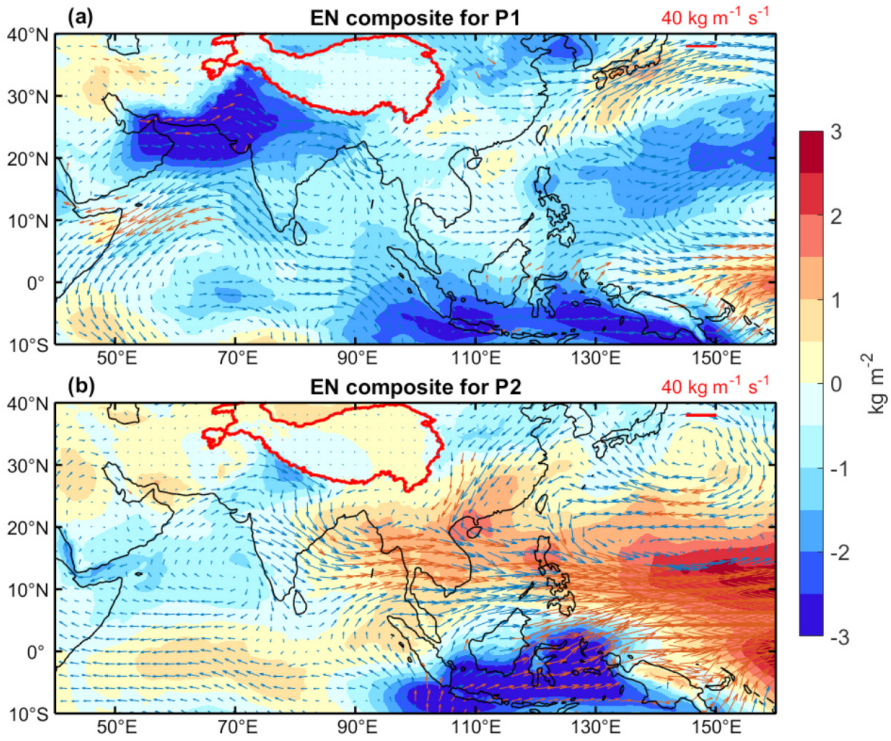

Figure 8. Composite of JJA(0) total column water vapor (shaded) and vertical integral of vapor flux (vector) anomalies for El Niño developing years including 1982–1983, 1997–1998, 2014–2016 events in the plateau monsoon region for the two periods. Significant water vapor flux anomalies at 90% confidence level are shown in red vectors.

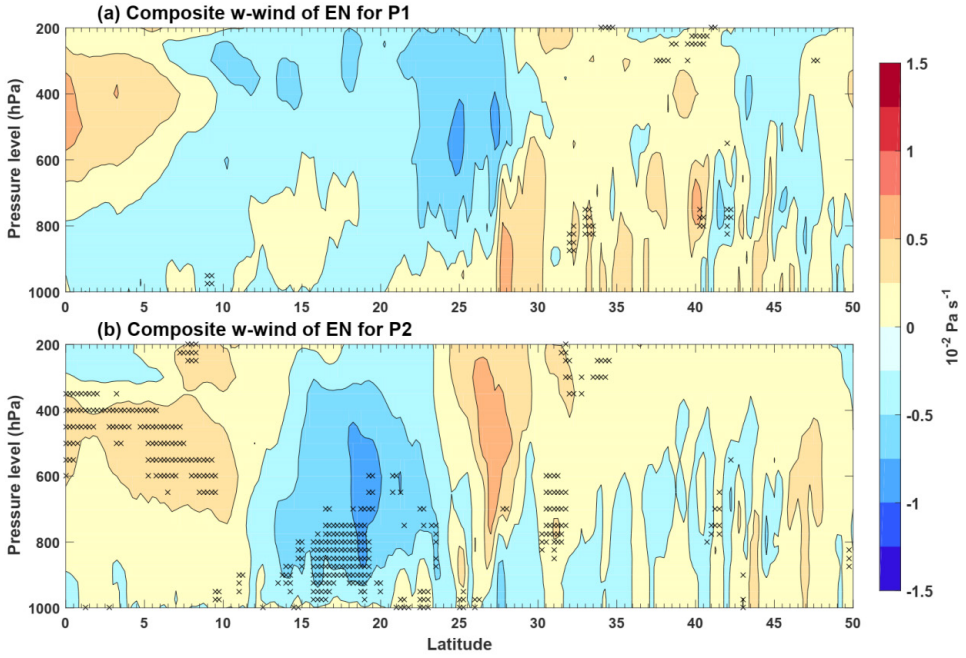

Figure 9. Latitude-pressure profile of composite JJA(0) vertical velocity (shaded) anomalies for El Niño developing years averaged in the longitude range of 80°–110°E for two sub-periods. The 'x' marked areas indicate composite vertical velocity anomalies exceed 90% confidence level. The negative values of vertical velocity indicate upward/ascent air motion, while the positive values indicate downward/subsidence motion.

the longitude range of 80°–110°E (from west to east of TP) for the two sub-periods, with latitude range from the equator to 50°N. There is no significant vertical motion at the south edge of TP (25°–30°N) in the former period, with anomalous upward motion at the south side of TP. In the later period, significant strong and deep anomalous upward motion can be seen at 15°–23°N, and, by contrast, anomalous subsidence motion appears at the south side of TP.

For changes on the longitude dimension, **Figure 10** shows the longitude-pressure profiles of composite anomalies of JJA(0) mean vertical velocity for El Niño developing years averaged in the latitude range of 27.5°–35°N (from south to north of TP) for the two sub-periods, with a longitude range of 60°–140°E. Distinct strong and deep downward motions can be seen at the western side (about 80°E) and eastern side (about 110°E) in the later period, indicating weakening of the water vapor flow climbing up to TP at both eastern and western.

5. Discussion and conclusions

In this study, we investigated the relationship between the variability of Tibetan Plateau summer precipitation and ENSO during the 1950–2019 period. The TP mean summer precipitation is significantly associated with the Niño-3.4 index, showing negative correlation coefficients from spring in the developing year to spring in the following year. However, such relations are unstable. Using a 21-year running correlation method, it is evident that the relation between the normalized TP mean summer precipitation and Niño-3.4 index has experienced an interdecadal change since the late 1980s, indicating that, for any 21-year window period after the late 1970s, the TP mean summer precipitation and Niño-3.4 index significantly correlate with each other. Both the CRU and ERA5 datasets support this point, and the mature phase winter Niño-3.4 index shows consistent results. Thus, we choose 1950–1978 (the

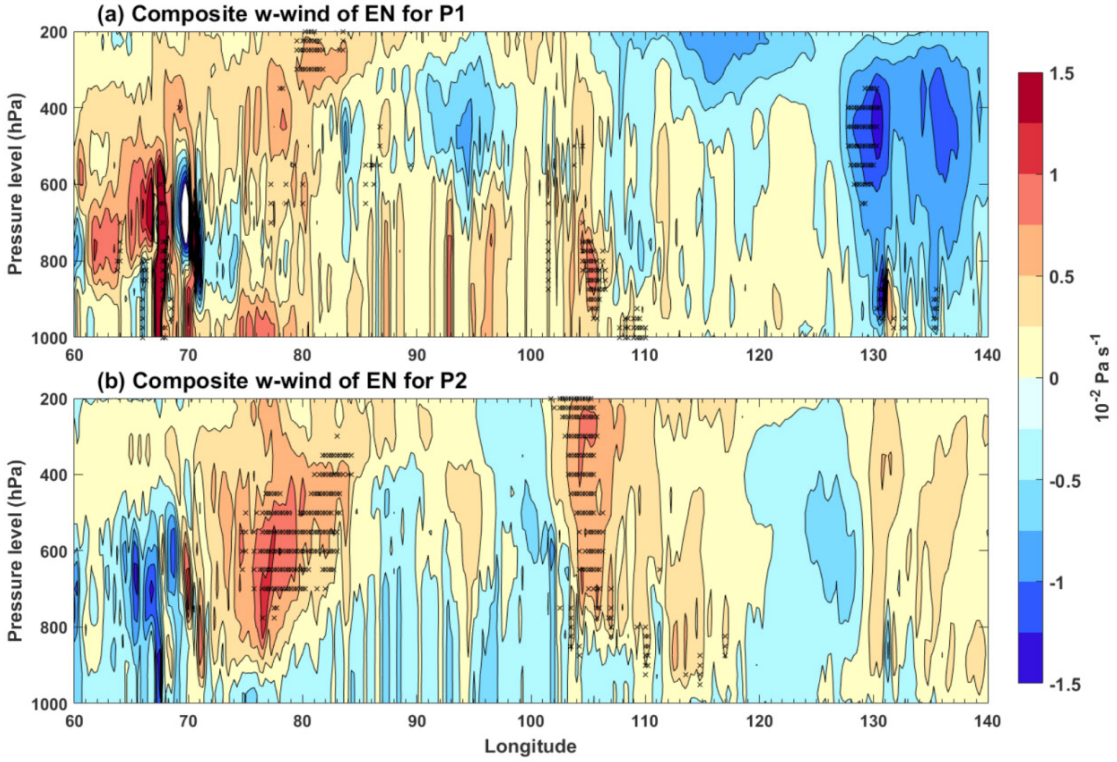

Figure 10. Same as Figure 9, but for the longitude-pressure profile averaged in the latitude range of 27.5°–35°N.

former period) and 1979–2019 (the latter period) as the two sub-periods to understand the different relationships between TP summer rainfall and tropical Indo-Pacific SST variabilities.

By analyzing the changes in ENSO intensity, ENSO pattern, moisture transport, and vertical motion in the two sub-periods, we discuss the possible mechanisms for the interdecadal change in the relationship between TP mean summer precipitation and Niño-3.4 index. Results show that, in the later period of 1979–2019, both the interdecadal strengthening of ENSO intensity and the SSTA patterns have an impact on the ENSO-induced TP summer precipitation anomalies. In the later period, significant anomalous water vapor flux appears in the Asia-Pacific region, with large amounts of water vapor being taken from the south and east of Asia, including the TP surrounding regions, to the tropical Pacific. Meanwhile, anomalous subsidence motion appears on the south side of TP. Distinct strong and deep downward anomalies can be seen at the western side and eastern side in the later period, indicating a weakening of the water vapor flow to TP.

For research on the Third Pole, this work is preliminary. We mainly present a result that the relations between TP summer precipitation and ENSO have experienced an interdecadal change since the late 1970s. How the strengthened ENSO amplitude influences the TP climate, and what role the central Pacific type of El Niño plays in modulating the climate over TP and the surrounding regions, needs further investigation. Another point is the role of the Indian Ocean during the El Niño developing stage [46]. Strong anomalous westward vapor fluxes can be seen in the Indian Ocean for the later period, and the season-dependent characteristic of SST anomalies in the Indian Ocean is not stable among the two sub-periods. In addition, the impact of local evaporation and evapotranspiration changes over TP on summer precipitation should also be investigated.

Author Contributions

All authors contributed to the study's conception and design. Material preparation, data collection and analysis were performed by Ning Cao, and Weinan Jiang. The first draft of the manuscript was written by Weinan Jiang and Ning Cao. Riga Aze and Jianjun Xu conceived and reviewed the manuscript and edited the text. Ning Cao and Jianjun Xu were responsible for the funding acquisition. All authors read and approved the final manuscript.

Conflict of Interest

The authors declare no conflict of interest.

Funding

This research was funded by the Second Tibetan Plateau Scientific Expedition and Research (STEP) program (2019QZKK0105), the Shenzhen Science and Technology Program (JCYJ20210324131810029), the National Natural Science Foundation of China (72293604, 42275017), the Guangdong Provincial College Innovation Team Project (060313452101), the Program for scientific research start-up funds of Guangdong Ocean University (R17056).

Acknowledgments

The authors acknowledge the teams from the University of East Anglia's Climatic Research Unit (CRU), the ECMWF, and the Hadley Centre for providing their data products. We extend our sincere thanks to the anonymous reviewers for their valuable constructive comments and suggestions, which have improved the quality of the manuscript.

References

[1] Yao, T., Liu, Y., Zhao, H., et al., 2011. Tibetan plateau. Encyclopedia of snow, ice and glaciers. Springer: Dordrecht. pp. 1172–1175. DOI: https://doi.org/10.1007/978-90-481-2642-2_578

[2] Qiu, J., 2008. China: The third pole. Nature. 454, 393–396. DOI: https://doi.org/10.1038/454393a

[3] Immerzeel, W.W., Van Beek, L.P.H., Bierkens, M.F.P., 2010. Climate change will affect the Asian Water Towers. Science. 328(5984), 1382–1385.
DOI: https://doi.org/10.1126/science.1183188

[4] Yao, T., Bolch, T., Chen, D., et al., 2022. The imbalance of the Asian water tower. Nature Reviews Earth & Environment. 3, 618–632.
DOI: https://doi.org/10.1038/s43017-022-00299-4

[5] Chen, F., Zhang, J., Liu, J., et al., 2020. Climate change, vegetation history, and landscape responses on the Tibetan Plateau during the Holocene: A comprehensive review. Quaternary Science Reviews. 243, 106444.
DOI: https://doi.org/10.1016/j.quascirev.2020.106444

[6] Jiang, X., Li, Y., Yang, S., et al., 2016. Interannual variation of summer atmospheric heat source over the Tibetan Plateau and the role of convection around the western maritime continent. Journal of Climate. 29(1), 121–138.
DOI: https://doi.org/10.1175/JCLI-D-15-0181.1

[7] He, C., Wang, Z., Zhou, T., et al., 2019. Enhanced latent heating over the Tibetan Plateau as a key to the enhanced East Asian summer monsoon circulation under a warming climate. Journal of Climate. 32(11), 3373–3388.
DOI: https://doi.org/10.1175/JCLI-D-18-0427.1

[8] Luo, X., Xu, J., Li, K., 2019. A review of atmospheric heat sources over Tibetan Plateau. Guangdong Ocean University. 39, 130–136. (in Chinese).

[9] Wang, X., Pang, G., Yang, M., 2018. Precipitation over the Tibetan Plateau during recent decades: A review based on observations and simulations. International Journal of Climatology. 38(3), 1116–1131.
DOI: https://doi.org/10.1002/joc.5246

[10] Joswiak, D.R., Yao, T., Wu, G., et al., 2013. Ice-core evidence of westerly and monsoon moisture contributions in the central Tibetan Plateau. Journal of Glaciology. 59(213), 56–66.
DOI: https://doi.org/10.3189/2013JoG12J035

[11] Yao, T., Masson-Delmotte, V., Gao, J., et al., 2013. A review of climatic controls on $\delta^{18}O$ in precipitation over the Tibetan Plateau: Observations and simulations. Reviews of Geophysics. 51(4), 525–548.
DOI: https://doi.org/10.1002/rog.20023

[12] Yao, T., Piao, S., Shen, M., et al., 2017. Chained impacts on modern environment of interaction between Westerlies and Indian monsoon on Tibetan Plateau. Bulletin of Chinese Academy of Sciences. 32(9), 976–984. (in Chinese).
DOI: https://doi.org/10.16418/j.issn.1000-3045.2017.09.007

[13] Li, G., Chen, H., Xu, M., et al., 2022. Impacts of topographic complexity on modeling moisture transport and precipitation over the Tibetan plateau in summer. Advances in Atmospheric Sciences. 39, 1151–1166.
DOI: https://doi.org/10.1007/s00376-022-1409-7

[14] Dong, N., Xu, X., Cai, W., et al., 2022. Comprehensive effects of interdecadal change of sea surface temperature increase in the Indo-Pacific Ocean on the warming-wetting of the Qinghai-Tibet Plateau. Scientific Reports. 12, 22306.
DOI: https://doi.org/10.1038/s41598-022-26465-8

[15] Jiang, X., F. Cai, Z. Li, et al., 2023. The westerly winds control the zonal migration of rainy season over the Tibetan Plateau. Communications Earth & Environment. 4, 363.
DOI: https://doi.org/10.1038/s43247-023-01035-6

[16] Klein, S.A., Soden, B.J., Lau, N., 1999. Remote sea surface temperature variations during ENSO: Evidence for a tropical atmospheric bridge. Journal of Climate. 12(4), 917–932.
DOI: https://doi.org/10.1175/1520-0442(1999)012<0917:RSSTVD>2.0.CO;2

[17] Xie, S., Kosaka, Y., Du, Y., et al., 2016. Indo-western Pacific Ocean capacitor and coherent climate anomalies in post-ENSO summer: A review. Advances in Atmospheric Sciences.

33, 411–432.
DOI: https://doi.org/10.1007/s00376-015-5192-6

[18] He, S., Yu, J., Yang, S., et al., 2020. ENSO's impacts on the tropical Indian and Atlantic Oceans via tropical atmospheric processes: Observations versus CMIP5 simulations. Climate Dynamics. 54, 4627–4640.
DOI: https://doi.org/10.1007/s00382-020-05247-w

[19] Wu, R., Zhu, P., 2021. Interdecadal change in the relationship of Indochina Peninsula May precipitation to ENSO. International Journal of Climatology. 41(4), 2441–2455.
DOI: https://doi.org/10.1002/joc.6968

[20] Ren, Q., Jiang, X., Shi, R., 2023. The enhanced relationship between summer rainfall over the eastern Tibetan Plateau and sea surface temperature in the tropical Indo-Pacific Ocean. Climate Dynamics. 60, 4017–4031.
DOI: https://doi.org/10.1007/s00382-022-06509-5

[21] Xie, S., Hu, K., Hafner, J., et al., 2009. Indian ocean capacitor effect on Indo-Western Pacific climate during the summer following El Niño. Journal of Climate. 22(3), 730–747.
DOI: https://doi.org/10.1175/2008JCLI2544.1

[22] Du, Y., Xie, S.P., Huang, G., et al., 2009. Role of air-sea interaction in the long persistence of El Niño-induced north Indian Ocean warming. Journal of Climate. 22(8), 2023–2038.
DOI: https://doi.org/10.1175/2008JCLI2590.1

[23] Chen, X., You, Q., 2017. Effect of Indian Ocean SST on Tibetan Plateau precipitation in the early rainy season. Journal of Climate. 30(22), 8973–8985.
DOI: https://doi.org/10.1175/JCLI-D-16-0814.1

[24] Park, J., Kug, J., Yang, Y., et al., 2023. Distinct decadal modulation of Atlantic-Niño influence on ENSO. npj Climate and Atmospheric Science. 6, 105.
DOI: https://doi.org/10.1038/s41612-023-00429-9

[25] Si, Y., Jin, F., Yang, W., et al., 2023. Change and teleconnections of climate on the Tibetan Plateau. Stochastic Environmental Research and Risk Assessment. 37, 4013–4027.
DOI: https://doi.org/10.1007/s00477-023-02492-3

[26] Nagura, M., Konda, M., 2007. The seasonal development of an SST anomaly in the Indian ocean and its relationship to ENSO. Journal of Climate. 20(1), 38–52.
DOI: https://doi.org/10.1175/JCLI3986.1

[27] Lei, Y., Zhu, Y., Wang, B., et al., 2019. Extreme lake level changes on the Tibetan Plateau associated with the2015/2016 El Niño. Geophysical Research Letters. 46(11), 5889–5898.
DOI: https://doi.org/10.1029/2019GL081946

[28] Hu, S., Zhou, T., Wu, B., 2021. Impact of developing ENSO on Tibetan plateau summer rainfall. Journal of Climate. 34(9), 3385–3400.
DOI: https://doi.org/10.1175/JCLI-D-20-0612.1

[29] Liu, M., Ren, H.L., Wang, R., et al., 2023. Distinct impacts of two types of developing El Niño-Southern oscillations on Tibetan plateau summer precipitation. Remote Sensing. 15(16), 4030.
DOI: https://doi.org/10.3390/rs15164030

[30] Ashok, K., Behera, S.K., Rao, S., et al., 2007. El Niño Modoki and its possible teleconnection. Journal of Geophysical Research. 112(C11).
DOI: https://doi.org/10.1029/2006JC003798

[31] Yeh, S., Kug, J., Dewitte, B., et al., 2009. El Niño in a changing climate. Nature. 461, 511–514.
DOI: https://doi.org/10.1038/nature08316

[32] Lee, T., McPhaden, M.J., 2010. Increasing intensity of El Niño in the central-equatorial Pacific. Geophysical Research Letters. 37(14).
DOI: https://doi.org/10.1029/2010GL044007

[33] Liu, Y., Cobb, K., Song, H., et al., 2017. Recent enhancement of central Pacific El Niño variability relative to last eight centuries. Nature Communications. 8, 15386.
DOI: https://doi.org/10.1038/ncomms15386

[34] Freund, M.B., Henley, B.J., Karoly, D.J., et al., 2019. Higher frequency of Central Pacific El Niño events in recent decades relative to past centuries. Nature Geoscience. 12, 450–455.

DOI: https://doi.org/10.1038/s41561-019-0353-3

[35] Li, G., Gao, C., Xu, B., et al., 2021. Strengthening influence of El Niño on the following spring precipitation over the Indochina Peninsula. Journal of Climate. 34(14), 5971–5984.
DOI: https://doi.org/10.1175/JCLI-D-20-0940.1

[36] Gao, C., Li, G., Chen, H., et al., 2020. Interdecadal change in the effect of spring soil moisture over the Indo-China Peninsula on the following summer precipitation over the Yangtze River Basin. Journal of Climate. 33(16), 7063–7082.
DOI: https://doi.org/10.1175/JCLI-D-19-0754.1

[37] Chen, L., Li, G., 2022. Interdecadal change in the relationship between El Niño in the decaying stage and the central China summer precipitation. Climate Dynamics. 59, 1981–1996.
DOI: https://doi.org/10.1007/s00382-022-06192-6

[38] Li, G., Gao, C., Lu, B., et al., 2021. Inter-annual variability of spring precipitation over the Indo-China Peninsula and its asymmetric relationship with El Niño-Southern Oscillation. Climate Dynamics. 56, 2651–2665.
DOI: https://doi.org/10.1007/s00382-020-05609-4

[39] Harris, I., Osborn, T.J., Jones, P., et al., 2020. Version 4 of the CRU TS monthly high-resolution gridded multivariate climate dataset. Scientific Data. 7, 109.
DOI: https://doi.org/10.1038/s41597-020-0453-3

[40] Hersbach, H., Bell, B., Berrisford, P., et al., 2023. ERA5 monthly averaged data on pressure levels from 1940 to present. Copernicus Climate Change Service (C3S) Climate Data Store (CDS).
DOI: https://doi.org/0.24381/cds.6860a573

[41] Hersbach, H., Bell, B., Berrisford, P., et al., 2020. The ERA5 global reanalysis. Quarterly Journal of the Royal Meteorological Society. 146(730), 1999–2049.
DOI: https://doi.org/10.1002/qj.3803

[42] Rayner, N.A., Parker, D.E., Horton, E.B., et al., 2003. Global analyses of sea surface temperature, sea ice, and night marine air temperature since the late nineteenth century. Journal of Geophysical Research. 108(D14).
DOI: https://doi.org/10.1029/2002JD002670

[43] Gong, Y., Li, T., Chen, L., 2020. Interdecadal modulation of ENSO amplitude by the Atlantic multi-decadal oscillation (AMO). Climate Dynamics. 55, 2689–2702.
DOI: https://doi.org/10.1007/s00382-020-05408-x

[44] Hong, C., Li, T., Ho, L., et al., 2010. Asymmetry of the Indian Ocean Basinwide SST Anomalies: Roles of ENSO and IOD. Journal of Climate. 23(13), 3563–3576.
DOI: https://doi.org/10.1175/2010JCLI3320.1

[45] Xu, X.D., Dong, L.L., Zhao, Y., et al., 2019. Effect of the Asian Water Tower over the Qinghai-Tibet Plateau and the characteristics of atmospheric water circulation. Chinese Science Bulletin. 64(27), 2830–2841. (in Chinese).

[46] Wu, X., Li, G., Jiang, W., et al., 2021. Asymmetric relationship between ENSO and the tropical Indian Ocean summer SST anomalies. Journal of Climate. 34(14), 5955–5969.
DOI: https://doi.org/10.1175/JCLI-D-20-0546.1